ELSEVIER

Contents lists available at ScienceDirect

## **Atmospheric Environment**

journal homepage: www.elsevier.com/locate/atmosenv





# Turbulent transport and reactions of plant-emitted hydrocarbons in an Amazonian rain forest

Jose D. Fuentes <sup>a,\*</sup>, Tobias Gerken <sup>a,1</sup>, Marcelo Chamecki <sup>b</sup>, Paul Stoy <sup>c</sup>, Livia Freire <sup>a</sup>, Jesus Ruiz-Plancarte <sup>a</sup>

- a Department of Meteorology and Atmospheric Science, The Pennsylvania State University, University Park, PA, USA
- <sup>b</sup> Department of Atmospheric and Oceanic Sciences, University of California, Los Angeles, CA, USA
- <sup>c</sup> Biological Systems Engineering, University of Wisconsin-Madison, Madison, WI, USA

#### HIGHLIGHTS

- Ozonolysis of rainforest emitted monoterpenes yielded hydroxyl radicals in amounts similar to the magnitude of light-dependent formation.
- Ozonelysis of monoterpenes produced concentrations of hydroxyl radicals similar the amounts consumed by the reaction with isoprene.
- · Monoterpenes and isoprene reactions with hydroxyl radical and ozone maintained an environment suitable to generate oxidants.

#### ABSTRACT

The processes governing the temporal and spatial patterns of isoprene and monoterpenes emitted by a rainforest in the central Amazon region of Brazil is investigated using a combination of field experiments and numerical simulations. Specifically, Large Eddy Simulations (LES) were used to resolve emissions of isoprene and monoterpenes, turbulent transport, and air chemistry. The coupled chemistry-transport LES included the effects of isoprene and monoterpenes reactivity due to reactions with hydroxyl radical and ozone. The LES results are used to compute vertically resolved budgets of isoprene and monoterpenes in the rainforest canopy in response to emissions, turbulent transport, surface deposition, and air chemistry. Results indicated that emission and dispersion dominated the isoprene budget as the gases were transported out of the canopy space. In a region limited by nitrogen oxides (with prevailing nitric oxide levels of < 0.5 parts per billion), the in-canopy chemical destruction removed approximately 10% of locally emitted monoterpenes. Hydroxyl radical production rates from the ozonolysis of monoterpenes amounted to  $\approx 2 \times 10^6$  radicals cm<sup>-3</sup> s<sup>-1</sup> and had similar magnitude to the light-dependent hydroxyl radical formation. One key conclusion was that the Amazonia rainforest abundantly emitted monoterpenes whose in-canopy ozonolysis yielded hydroxyl radicals in amounts similar to the magnitude of light-dependent formation. Reactions of monoterpenes and isoprene with hydroxyl radical and ozone were necessary for the maintenance of the Amazon rainforest canopy as a photochemically active environment suitable to generate oxidants and secondary organic aerosols.

## 1. Introduction

The Amazon rainforest represents the most expansive and contiguous region of the world with the largest and the most diverse emissions of biogenic volatile organic compounds (BVOCs) (Jardine et al., 2011, 2015a,b). Due to the suitable environmental conditions to promote productive biosynthesis and emissions – namely high air temperature (> 20 °C) and sunlight – the rainforest releases isoprenoid molecules year round (Arneth et al., 2011; Sindelarova et al., 2014). Plants in the Amazon emit rich blends of BVOCs that are mostly comprised of isoprene ( $C_5H_8$ ), monoterpenes ( $C_{10}H_{16}$ ), sesquiterpenes ( $C_{15}H_{24}$ ), and oxygenated compounds such as methanol ( $CH_3OH$ ) (Jardine et al., 2011,

2015a). Because of strong sources, isoprene and monoterpenes can reach maximum ambient mixing ratios of 20 and 2 parts per billion (ppb) on a volume basis, respectively, with some seasonality in emissions due to foliage ontogeny (Alves et al., 2016; Wei et al., 2018; Yáñez-Serrano et al., 2018).

In the tropical atmospheric boundary layer (ABL) overlying the rainforest, the observed large hydroxyl radical (HO) reactivities arise from the abundant emissions of BVOCs (Edwards et al., 2013; Nölscher et al., 2016a,b; Pfannerstill et al., 2021). In response to the pletora of emitted reactive chemical species, the HO budget in the ABL is adjusted by BVOC levels (Liu et al., 2016, 2018). This influence occurs because the principal sink of isoprene is its reaction with HO. The oxidation of

E-mail address: idfuentes@psu.edu (J.D. Fuentes).

 $<sup>^{\</sup>ast}$  Corresponding author.

<sup>&</sup>lt;sup>1</sup> Current address: School of Integrated Sciences, James Madison University, Harrisonburg, VA, USA

isoprene generates hydroperoxy aldehydes (HPALD) whose rapid photolysis results in a first-generation of hydroperoxyl radical (HO2) and HO (Taraborrelli et al., 2012; Fuchs et al., 2013; Rohrer et al., 2014; Bates and Jacob, 2019; Schwantes et al., 2020). In addition, ozonolysis of monoterpenes (Atkinson et al., 1992; Aschmann et al., 2002; Herrmann et al., 2010) produces relatively high yields of HO, thereby contributing to the oxidation capacity of the tropical ABL (Lelieveld et al., 2008; Whalley et al., 2011). In general, the reactions of BVOCs with ozone (O<sub>3</sub>), HO, and nitrate radical (NO<sub>3</sub>) contribute to the formation of additional oxidants (e.g., organic peroxide radicals) and secondary organic aerosols (SOAs) (Fuentes et al., 2000; Pöschl et al., 2000, 2010). Therefore, BVOCs can indirectly play critical roles in cloud formation processes (Pöschl et al., 2010) and regional climate (Barr et al., 2003). Despite the recent progress in discerning the chemical cycles of BVOCs, additional investigations are still required to determine (i) the mechanisms governing their turbulent transport from the biosphere to the ABL and (ii) the ensuing chemistry under the influences of varying levels of nitrogen oxides (NOx).

Turbulence is the primary agent transporting BVOCs and associated chemical processes occurring within and above the rainforest canopy. During the daytime, only the upper half of the rainforest canopy is well mixed whereas its lower region is either partially or poorly mixed due to the effective momentum sink in the forest crown (Fitzjarrald et al., 1990; Kruijt et al., 2000; Gerken et al., 2017). For the most part, the rainforest canopy remains poorly mixed at night due to buoyancy destruction of mechanically produced turbulence (Fitzjarrald and Moore, 1990; Santos et al., 2016; Freire et al., 2017). Turbulence characteristics give rise to median canopy residence times that can approach 30 min in the lower canopy layers under statically neutral conditions (Gerken et al., 2017). Because such air parcel residence times are comparable to lifetimes of many BVOCs (Fuentes et al., 2000), appreciable amounts can undergo reactions before they are vented out of the forest environment. Furthermore, the transport of BVOCs is impacted by sweeps and ejections from coherent mixing-layer eddies (Raupach et al., 1996; Finnigan, 2000) whose penetration depth into the canopy is limited by the dense Amazon plant canopy (Fitzjarrald et al., 1990; Kruijt et al., 2000). The need to explore turbulent transport and chemistry in concert is further highlighted as air parcels emanating from the canopy are enriched with plant-emitted hydrocarbons as descending air motions transport O<sub>3</sub> and other atmospheric oxidants into the canopy airspace (Fuentes et al., 2007; Gerken et al., 2016; Freire et al., 2017).

Large Eddy Simulations (LES) can provide realistic estimates of the links between the turbulence features in both the plant canopy and the atmospheric boundary layer, and the chemistry of isoprene and monoterpenes, which are ordinarily under resolved in most regional models. Early LES studies involving plant canopies applied to passive scalars (Shaw and Schumann, 1992; Edburg et al., 2011) and treated reactive gases (Patton et al., 2001) based on their exponential decays due to chemical reactions. Recent LES investigations coupled condensed (Vilà-Guerau de Arellano et al., 2011; Ouwersloot et al., 2013) and detailed (Su et al., 2016; Khan et al., 2021) photochemical mechanisms with atmospheric turbulence to determine the oxidation of isoprene in convective boundary layers, but did not include in-canopy chemical reactions. Patton et al. (2016) integrated canopy and convective boundary-layer processes to link turbulence and scalars, emphasizing the potential to extend the LES approach to include photochemical mechanisms necessary for studying detailed chemical reactions of BVOCs in forest canopies. In addition, stochastic Lagrangian transport models (Strong et al., 2004; Rinne et al., 2012) have been applied to determine the reactions isoprene and monoterpenes with oxidants as first order decay in and above forest canopies.

Building on these earlier studies, this investigation was framed around three objectives. First, we determined the processes governing temporal and spatial patterns of isoprene and monoterpenes in response to emissions, turbulent transport, surface dry deposition, and chemical reactions. Second, we estimated the fraction of locally emitted isoprene

and monoterpenes destroyed in the rainforest canopy due to surface deposition and chemical reactions occurring under the influences of observed  $\rm O_3$  and nitric oxide (NO) levels. Third, given the substantial daytime concomitant emissions of isoprene and monoterpenes in the rainforest, we ascertained the feedback generated between ozonolysis of monoterpenes and chemical destruction of isoprene via its reaction with HO. To achieve these objectives, we included in an updated LES the algorithm for the explicit treatment of chemical reactions to resolve turbulent transport of mass, energy, and momentum in and above a rainforest canopy.

#### 2. Methodology

#### 2.1. Study site description and field measurements

Field data used here were collected during April 2014 to January 2015 (Fuentes et al., 2016). The study site is located approximately 60 km north-northwest of Manaus, Amazonas, Brazil. The site consists of dense primary rainforest with a canopy height  $(h_c)$  of approximately 35 m. The leaf area index (LAI) ranged from 5.7 to 7.3 m<sup>2</sup> m<sup>-2</sup> (McWilliam et al., 1993; Marques Filho et al., 2005; Tota et al., 2012), depending on the location of measurements. Terrain consists of gentle valleys and hills. A 50-m meteorological tower is located on an approximately 60-m high plateau. Located in the middle of the forest, the tower served as the platform to mount nine triaxial sonic anemometers (CSAT-3, Campbell Scientific Inc, Logan, UT) to measure the three wind components (u, v, v)and w), their turbulent fluctuations, and the sonic temperature at 20 Hz. Measurement heights were  $zh_c^{-1} = 1.38, 1.15, 1.0, 0.90, 0.70, 0.63,$ 0.52, 0.39, and 0.20. One additional sonic anemometer was placed near the tower at  $z h_c^{-1} = 0.04$ . Mean air relative humidity and temperature (HMP-155, Vaisala, Vantaa, Finland) were measured at the 32-m height. Ambient O<sub>3</sub> mixing ratios (49i, Thermo Fisher Scientific, Waltham, MA) were measured at a frequency of 1 Hz. A Proton Transfer Reaction Mass Spectrometer (PT-RMS, Ionicon Analytik, Innsbruck, Austria) measured isoprene, aggregated monoterpene, and the sum of methyl-vinyl ketone and methacrolein (MVK + MACR) mixing ratios. Both instruments shared a common gas sampling inlet equipped with a rain-shield and placed at  $zh_c^{-1} = 1.14$  and were housed in a temperature-controlled shed, located 5 m from the tower. Air samples were drawn at a rate of 12 L min<sup>-1</sup> through a 1- $\mu$  m pore size Teflon filter and through a 3/8-inch outer diameter Teflon tube that was shielded from sunlight. Photosynthetically active radiation (PAR) was measured at  $zh_c^{-1}$  = 1.46, and air temperature was recorded at  $zh_c^{-1} = 1.46, 1.21, 0.8, 0.44,$ 0.15. Ambient air pressure as well as turbulent fluxes of sensible and latent heat  $(z h_c^{-1} = 1.46)$  were averaged in 30-min intervals. Additional details on the study site, measurements, and postprocessing of data are provided elsewhere (Fuentes et al., 2016).

#### 2.2. Large eddy simulation

A description of the governing equations and the main features of the LES are provided here and additional details are reported elsewhere (Chamecki et al., 2008, 2009; Pan et al., 2014). For incompressible flows ( $\nabla \cdot \widetilde{\mathbf{u}} = 0$ ), the filtered momentum and air mass conservation equations were solved to obtain the three dimensional wind field ( $\widetilde{\mathbf{u}}$ ):

$$\frac{\partial \widetilde{\mathbf{u}}}{\partial t} + (\widetilde{\mathbf{u}} \cdot \nabla) \widetilde{\mathbf{u}} = -\frac{1}{\rho} \nabla (\widetilde{p} + P) - \mathbf{g} \left( \frac{\widetilde{\theta}_{v} - \langle \widetilde{\theta}_{v} \rangle}{\langle \widetilde{\theta}_{v} \rangle} \right) - \nabla \overline{r}_{sgs} - \mathbf{d}.$$
 (1)

Terms on the right hand side of Equation (1) represent the resolved pressure gradient force, buoyancy force, subgrid-scale (SGS) force, and the drag force exerted by the forest canopy (represented as a porous medium with negligible fractional solid volume). Hereafter,  $\rho$  is air density,  $\widetilde{p}$  is resolved modified pressure (as it also includes the SGS turbulent kinetic energy), P is the mean pressure used to impose a mean

pressure gradient to drive the flow,  $\tilde{\theta}_v$  is virtual potential temperature, **g** is the gravitational acceleration,  $\tau_{\text{SgS}}$  is the SGS stress tensor, and angle brackets indicate average over horizontal planes. Following Shaw and Schumann (1992), the canopy drag (**d**) was determined as

$$\mathbf{d} = C_d \ (\mathbf{P} \ a(z)) \cdot (|\widetilde{\mathbf{u}}|\widetilde{\mathbf{u}}), \tag{2}$$

where  $C_d$  is a constant drag coefficient (form drag), **P** is a diagonal tensor that projects the total leaf area density onto planes perpendicular to each of the three spatial dimensions (Pan et al., 2014), and a(z) is the plant area density assumed to be reasonably approximated by the leaf area density. This study assumed a random orientation of leaves ( $P_x = P_y = P_z = 1/2$ ) and a horizontally homogeneous distribution of LAI for each layer with  $C_d = 0.4$ . The temporal change of virtual potential temperature  $\widetilde{\theta}_v$  was expressed as a filtered advection-diffusion equation

$$\frac{\partial \widetilde{\theta}_{v}}{\partial t} + \nabla \cdot \left( \widetilde{\mathbf{u}} \, \widetilde{\theta}_{v} \right) = - \, \nabla \pi_{\theta_{v}} + H, \tag{3}$$

where  $\pi_{\theta_{\nu}}$  is the SGS buoyancy flux, and H is a source term representing the total buoyancy flux from the forest canopy to overlying air layers. Similarly, filtered advection-diffusion-reaction equations were solved for each gaseous chemical species,  $\widetilde{\gamma}_{i}$ 

$$\frac{\partial \widetilde{\chi_i}}{\partial t} + \nabla \cdot (\widetilde{\mathbf{u}} \widetilde{\chi_i}) = - \nabla \pi_{\chi_i} + C_i + E_i - D_i, \tag{4}$$

where  $\pi_{\gamma_i}$  is the SGS flux for the chemical species,  $C_i$  represents the gas net loss or gain due to chemical reactions, and  $E_i$  and  $D_i$  represent gas emission and deposition, respectively. The filtered equations were closed through SGS momentum fluxes that were determined using the scale dependent Lagrangian dynamic Smagorinsky model (Bou-Zeid et al., 2004). Scalar SGS-fluxes were estimated based on the SGS eddy viscosity and a constant SGS Schmidt number ( $Sc_{\tau} = 0.8$ ). Equations (1) and (3) were discretized using a pseudo-spectral approach in the horizontal directions and a second-order centered finite-difference scheme in the vertical. Equations for the gases were discretized using the finite volume method with the third-order upwind advection scheme SMART (Gaskell and Lau, 1988). The time integration of the LES was advanced through the second-order Adam-Bashforth scheme (Peyret and Taylor, 2012). Lateral boundary conditions were periodic for momentum and all scalars. The upper boundary condition was no-stress/no-flux while a wall model based on Monin-Obukhov similarity (Foken, 2006) was used for the lower boundary condition situated at the forest floor.

## 2.2.1. Emissions of biogenic hydrocarbons

The Model of Emissions of Gases and Aerosols from Nature (MEGAN) version 2.1 (Guenther et al., 2012) was used to estimate emissions of isoprene and monoterpene as a function of leaf area density, temperature, and PAR in the canopy. Vertically resolved emissions ( $E_i(z)$ ) for a given gas species (i) were estimated for each plant functional type using (Guenther et al., 2006):

$$E_i(z) = C_{ce} \, \varepsilon_i \, \gamma_P(z) \, \gamma_T(z) \, \gamma_A \, \gamma_{SM} \, \gamma_{CO}, \, a(z). \tag{5}$$

In Equation (5),  $C_{\rm ce}$  is a canopy environment model dependent factor (here  $C_{\rm ce}=0.17$  is adopted to adjust emissions to observed ambient gas levels (Kuhn et al., 2007; Karl et al., 2007)),  $\varepsilon_i$  is a plant species specific emission factor. The  $\gamma_P(z)$  and  $\gamma_T(z)$  functions consider the influences of PAR and temperature on emissions of isoprene and monoterpenes. As documented by previous field studies (Rinne et al., 2002; Kuhn et al., 2002; Jardine et al., 2015a), in the Amazon emissions of monoterpenes also depend on PAR levels. The activity factors of leaf age  $(\gamma_A)$ , soil moisture  $(\gamma_{SM})$ , and carbon dioxide inhibition on hydrocarbon emissions  $(\gamma_{CO_2})$  were assumed to equate unity as done by Alves et al. (2016). The vertically resolved temperature and PAR functions,  $\gamma_T(z)$  and  $\gamma_P(z)$ , modulating basal emissions were calculated following Equations 3–11 in Guenther et al. (2012). A two-stream radiative transfer

module (Sellers, 1985; Gu, 1999; Moon et al., 2020) was used to estimate PAR for shaded and sunlit leaves. Fractions of sunlit leaves were determined assuming exponential decreases in such foliage with cumulative leaf area as in Dai et al. (2004). Basal emission of isoprene was based on  $\varepsilon_{\rm Iso}=7.0$  mg m $^{-2}$  h $^{-1}$  and emissions of monoterpenes were calculated as the sum of eight monoterpenes listed in the MEGAN formulation (Guenther et al., 2012) and identified in the studied forest canopy (Jardine et al., 2015a). Emission profiles (Fig. 1) were calculated using Equation (5) every 30 min during the day and linearly interpolated for times in between. To avoid the repeated execution of the canopy radiative transfer algorithm within the LES, the BVOC emissions were computed offline and externally imposed on the LES.

#### 2.2.2. Summary of reactions involving isoprene and monoterpenes

The third research objective was achieved by estimating the oxidation of isoprene and monoterpenes in and above the rainforest canopy, utilizing a condensed photochemical mechanism (Table S1). Based on the initial gas concentrations, the mechanism calculates formation and destruction of HO, NO<sub>3</sub>, and O<sub>3</sub> due to photooxidation of BVOCs. The HO initiates the oxidation of isoprene (ISOP) and monoterpenes (MON), resulting in the formation of peroxyl radicals (RO<sub>2</sub>, TPO<sub>2</sub>), R9 and R28. As done in previous studies (e.g., Van Stratum et al., 2012), the reaction of ISOP with O3 is not included in the chemical mechanism due to the extremely reaction coefficient  $(k_{O_{3,Iso}} \, = \,$  $10^{-17}\,\text{cm}^3\,\text{molec}^{-1}\,\text{s}^{-1}).$  Monoterpenes also react with NO $_3$  to form free radicals (TPO2), R30. The ozonolysis of monoterpenes generates HO, methyl vinyl keone (MVK), and hydroperoxyl radicals (HO2), see R29 in Table S1. The RO2 and TPO2 are short-lived and in the presence of NO can produce NO2, HO2, MVK, HO, and formaldehyde (CH2O), R15 and R31. Additional reactions involving MVK with HO generate HO2 and CH<sub>2</sub>O, R10, which can undergo photolysis to generate HO<sub>2</sub>, R6. Also, the reaction of CH2O with HO produces HO2, R16, which subsequently combines with NO to generate HO plus NO<sub>2</sub>. In low-NO environments (i. e., [NO] < 30 parts per trillion (ppt)), the HO<sub>2</sub> can react with O<sub>3</sub> to form HO whereas the reaction of HO2 with NO dominates and produces HO and NO<sub>2</sub> in NO-laden air masses (Atkinson, 2000). The photolysis of NO<sub>2</sub> generates NO and ground-triplet state atomic oxygen (O(<sup>3</sup>P)), which readily combines with O<sub>2</sub> to produce O<sub>3</sub>, R5. Therefore, this summary of reactions (R9 to R34) indicates that one key role of BVOCs is to convert NO to NO2, which is the key precursor of O3. The condensed photochemical mechanism (Table S1) is an enhanced version of the one described in Heus et al. (2010) and tested for isoprene chemistry in numerical simulations applied above the Amazon rainforest (Vilà-Guerau de Arellano et al., 2011). The isoprene mechanism is based on the one reported by Geiger et al. (2003) and Ouwersloot et al. (2013). Monoterpenes are represented as a single chemical species as implemented in the Model for Ozone and Related chemical Tracers (MOZART) version 4 (Emmons et al., 2010) and used by Su et al. (2016). An implicit two-step chemical solver is applied to estimate rates of reactions (Verwer, 1994; Verwer and Simpson, 1995). Vilà-Guerau de Arellano et al. (2011) and Su et al. (2016) reported that equilibrium HO concentrations in the current chemical mechanism are 30-50% higher than in the more complete chemical mechanisms due to the unaccounted NO<sub>x</sub> sinks in species such organic nitrates (RONO2).

#### 2.3. Numerical simulation setup

The modeling domain was  $3584 \times 1792 \times 1120$  m<sup>3</sup> and was discretized by  $164 \times 82 \times 320$  grid points in the streamwise, crosswise, and vertical direction, respectively. The vertical resolution was set as  $\Delta z = 3.5$  m, which yielded ten layers in the canopy. The horizontal model resolution was  $\Delta x = \Delta y = 21.85$  m, which corresponded to an aspect ratio of  $\Delta x/\Delta z = 2\pi$ . The simulation time step was 0.04 s and the chemical mechanism was called every 8 simulation steps. The Coriolis effect was neglected due to the field site's proximity to the Equator. The

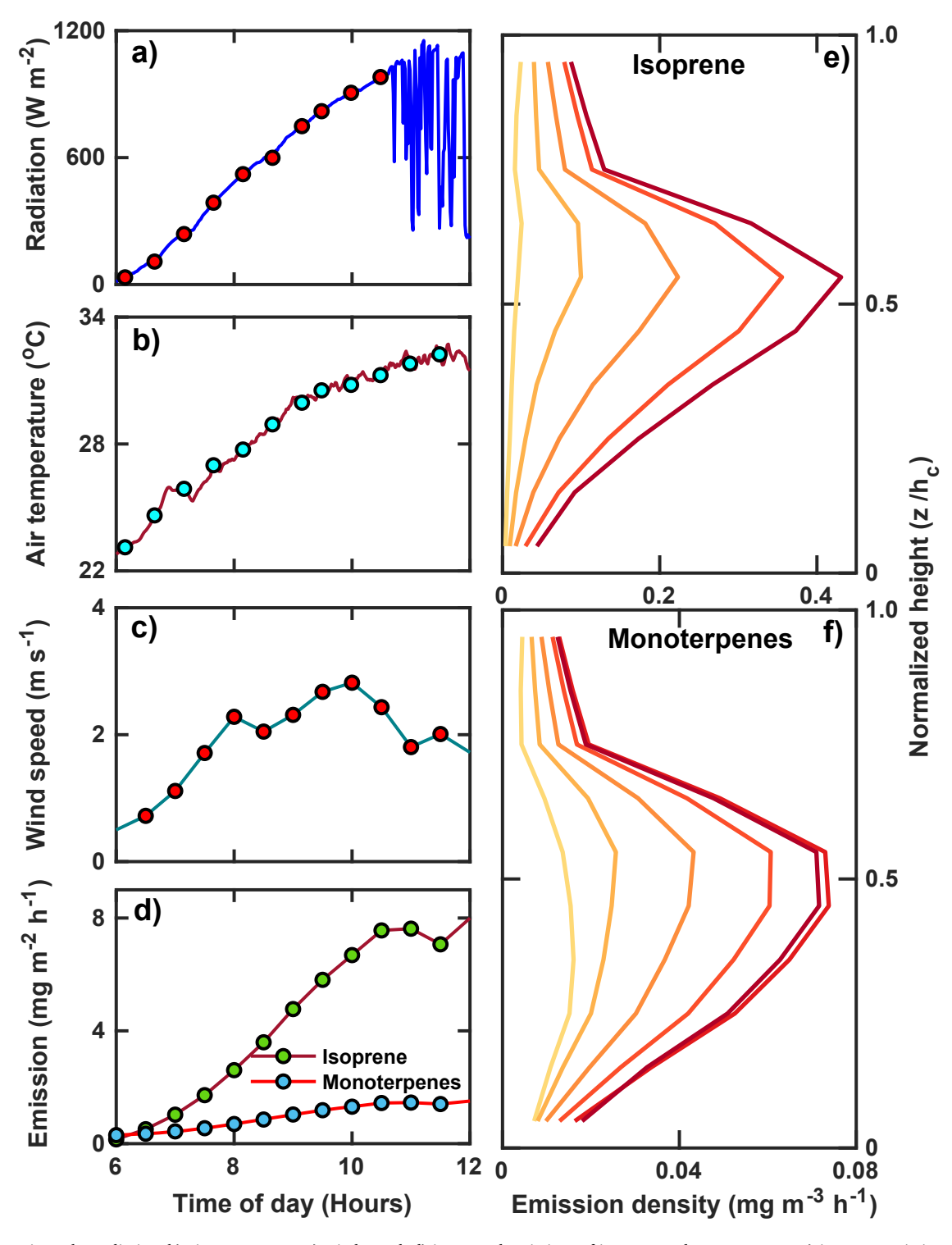


Fig. 1. a) Incoming solar radiation, b) air temperature, c) wind speed, d) integrated emissions of isoprene and monoterpenes, e) isoprene emission density, and f) monoterpene emission density from 6:00 h to 12:00 h (yellow to dark red) on September 14, 2014. Shaded circles represent select times when data are plotted. (For interpretation of the references to colour in this figure legend, the reader is referred to the Web version of this article.)

LAI was set to 6.0 using the vertical leaf area distribution measurements (Tota et al., 2012). Simulations were forced by imposing time dependent mean pressure gradient and heat sources designed to match observed conditions. Simulations from 6:00 h (sunrise) to 12:00 h (all times are given in local time) on September 21, 2014 are included in this manuscript. After sunrise, the pressure gradient driving the flow increased so that diurnal cycle of the friction velocity (u\*) at the canopy top closely matched observed values. The mean pressure gradient was determined

from the mean force balance  $dP/dx = \rho u_*^2/Z_i$  ( $Z_i$  is the depth of the convective boundary layer). Due to the time lag required for the flow field to respond to changes in the pressure gradient forcing, the time evolution of the forcing had to be adjusted (see Supplement for details). Vertically-resolved kinematic heat fluxes  $(\overline{w'}\overline{\theta_{\nu}})$  from eddy covariance measurements were temporally smoothed (using a linear fit) and vertically interpolated to the numerical grid levels to produce buoyancy fluxes,  $B_{\rm smooth}(z, t)$ . In the lower half of the canopy  $(z/h_c < 0.5)$  fluxes

were set to zero as observed daytime fluxes were negligible. The heat source, H, in Equation (3) was specified as  $H(z, t) = B_{\text{smooth}}(z, t)/dz$ . Similarly to H, the in-canopy water vapor source was specified assuming a constant Bowen ratio in the vertical as determined from above-canopy measurements (Fuentes et al., 2016).

Upper air sounding data taken at a site 20 km away from the tower were used to initialize the LES. The  $\theta_{\nu}$  profile was constant for the first 50 m above ground and then  $\theta_{\nu}$  increased by the gradient of  $\partial \theta_{\nu}/\partial z =$ 0.024 K m<sup>-1</sup> between 50 and 150 m and  $\partial\theta_{\nu}/\partial z = 0.016$  K m<sup>-1</sup> above 150 m. The initial surface temperature was set to 299 K and the specific humidity profile was set to 17.0 g kg<sup>-1</sup> below 150 m and 13.0 g kg<sup>-1</sup> above 150 m. Ozone levels were initialized at 8 ppb at the surface and then linearly increased by 0.056 ppb m<sup>-1</sup> until they reached a constant level above 450 m. Concentrations of chemical species were initialized as constant values within the entire domain (a value of zero was chosen unless indicated in Table 1). Due to the unpolluted conditions at the study site, NO<sub>2</sub> was set to 0.1 ppb with 0.1 ppb of NO near the surface. The soil NO source of  $5 \times 10^{-4}$  ppb m s<sup>-1</sup> was considered (Vilà-Guerau de Arellano et al., 2011). Ozone deposition to the canopy was modeled following Wolfe and Thornton (2011). Isoprene deposition to the ground surface was considered through a deposition velocity,  $V_{\rm dep} = 2.7 \, \rm mm \, s^{-1}$ (Gordon et al., 2014). At the ground, zero flux of monoterpenes was assumed. Three numerical simulations were performed. The first simulation (hereafter labeled as Iso) included emissions and chemistry of isoprene only (R1 - R27, Table S1). The Iso scenario was done to separate the influences of isoprene sinks associated with HO production from ozonelysis of monoterpnes. There are monoculture forested ecosystems that only emit isoprene (Fuentes et al., 1999). The second simulation combined isoprene and monoterpenes (Mon), R28 - R34. In this simulation, monoterpenes were represented by a single chemical species whose reactivity  $(k_{O_{3.Mono}} = 1.82 \times 10^{-16} \, \text{cm}^3 \, \text{molec}^{-1} \, \text{s}^{-1})$  was calculated as the weighted geometric mean of the composition of monoterpenes observed at the study site (Jardine et al., 2015a). The third simulation (Pin) assumed that the emitted monoterpenes had the reactivity of  $\alpha$ -pinene ( $k_{\rm O_3\,Pin}=8.09\times10^{-17}\,cm^3\,molec^{-1}\,s^{-1}$ ) as assumed in other atmospheric chemistry models (Emmons et al., 2010). Finally, for the purposes of assessing the importance of chemistry versus transport of monoterpenes, non-reactive tracers were also included in the simulations. These were referred to as passive monoterpenes ( $Mon_{Pas}$ ), but their emission and deposition were estimated in the same manner as the reactive chemical species.

### 2.4. Fluxes and budgets of isoprene and monoterpenes

The LES results were analyzed for the canopy region  $(0 \le z \le h_c)$ . Average gas mixing ratios within the canopy volume were obtained from Equation (4) by calculating averages over horizontal planes (temporal averages were also obtained over periods of 10 min). Resulting averages were vertically integrated to derive the change of gas mixing ratio with time  $\left(\frac{d\langle \widetilde{y_j}\rangle_{\rm Can}}{dt}\right)$ , given by

**Table 1**Data used to initialize the vertical profiles in the LES domain.

| Variable   | Height                 | Value                            | Unit                 |
|--|------------------------|----------------------------------|----------------------|
| $\theta_{\nu}$                                     | $z \le 50$             | 299.1                            | K                    |
| $\Delta \theta_{\nu}/\Delta z$                     | $50~m < z \leq 150~m$  | 0.024                            | ${ m K~m}^{-1}$      |
| $\Delta \theta_{ m \scriptscriptstyle V}/\Delta z$ | z > 150  m             | 0.016                            | ${ m K}~{ m m}^{-1}$ |
| q  | $z \leq 150$           | 17.0                             | ${ m g~kg^{-1}}$     |
|  | z > 150                | 13.0                             | ${ m g~kg^{-1}}$     |
| $O_3$  | $z \leq 450 \text{ m}$ | $8 + 0.056 \text{ ppb m}^{-1} z$ | ppb                  |
|  | z > 450  m             | 33.1                             | ppb                  |
| NO   | $z \leq 150 \text{ m}$ | 0.1                              | ppb                  |
| $NO_2$   |                        | 0.1                              | ppb                  |
| CH <sub>4</sub>                                    |                        | 1724.0                           | ppb                  |

$$\frac{d\langle \widetilde{\chi_j} \rangle_{\text{Can}}}{dt} = \frac{1}{h_c} \left[ -F_j(h_c) + E_{j,\text{Can}} - D_{j,\text{Can}} + C_{j,\text{Can}} \right]. \tag{6}$$

Here  $\langle \widetilde{\chi_j} \rangle_{\rm Can} \equiv h_c^{-1} \int_0^{h_c} \langle \widetilde{\chi_j} \rangle_{xy} \, dz$  is the mean gas mixing ratio inside the canopy,  $\langle \widetilde{\chi_j} \rangle_{xy}$  is the horizontally-averaged mixing ratio,  $F_j(h_c)$  is the total gas flux at the top of the canopy (including contributions from resolved and SGS fluxes). The hydrocarbon flux at the surface was assumed to be zero. The isoprene surface deposition was prescribed as  $V_{\rm dep} = 2.7$  mm s<sup>-1</sup> (Gordon et al., 2014; Nguyen et al., 2015) and the deposition of monoterpenes was set to zero.

#### 3. Results and discussion

#### 3.1. Canopy emissions of isoprene and monoterpenes

During the rainy season in the central Amazon, prevailing atmospheric conditions from sunrise to local noontime kept recurring day after day. Afternoons became predominantly cloudy and rainfall events mostly occurred during 14:00 to 16:00 local h (Fuentes et al., 2016; Vilà-Guerau de Arellano et al., 2020). Because the principal goal of this study was to estimate the in-canopy oxidation rates of isoprene and monoterpenes, the numerical model simulations focused on a representative day (September 14, 2014) during the start of the rainy season. Sunny conditions dominated the period of the numerical simulations, with maximum incoming solar irradiance reaching nearly 1200 W m<sup>-2</sup> around 11:00 h. Clouds appeared around 11:00 h and reduced the incoming sunlight levels during the last hour of simulations (Fig. 1a). Air temperature varied from 23 (at 6:30 h) to 32 °C (at 12:00 h) while wind speed remained below 3.5 m s<sup>-1</sup> (Fig. 1b and c). Computed emissions of isoprene and monoterpenes increased after sunrise and reached values of 8.0 and 1.5 mg m $^{-2}$  h $^{-1}$  at 12:00 h (Fig. 1d), respectively. Emission rates (Fig. 1d) were in good agreement with previously reported canopy-scale fluxes in the central Amazonia region (Rinne et al., 2002; Kuhn et al., 2007). Isoprene emission density profiles changed rapidly with canopy depth (Fig. 1e), reaching maximum values of 0.4 mg m<sup>-3</sup>  $h^{-1}$  around 12:00 h at z  $h_c^{-1} = 0.6$  where the greatest amount of active biomass was present and most PAR interception occurred. As emissions of monoterpenes were dependent of PAR, the bulk of emissions originated from deeper in the forest canopy (z  $h_c^{-1} > 0.4$ ), with maximum emission density values of 0.075 mg m<sup>-3</sup> h<sup>-1</sup> (Fig. 1f).

The thermodynamic conditions of the convective ABL exerted control on the vertical distribution of isoprene and monoterpenes. The LESchemistry coupled model provided high-resolution temporal Z<sub>i</sub> variations. Under the assumed atmospheric thermodynamic conditions, simulated  $Z_i$  rapidly changed over the course of the morning hours and  $Z_i$ values ranged from 200 m at 8:00 h to approximately 760 m at 12:00 h (Fig. 2 a). Simulated  $Z_i$  values at 11:00 h and 14:00 h were comparable to mixed layer depths of 491  $\pm$  133 m and 813  $\pm$  128 m, respectively, observed 24 km away from the study site during the wet season (Fisch et al., 2004). Additional details on the atmospheric boundary layer thermodynamic evolution as well as turbulence statistics are provided in the Supplement (Figs. S1–S4). Meanwhile, canopy emissions of isoprene and monoterpenes contributed to rapid increases in mixing ratios of the gases in the convective boundary layer. Most of the emitted hydrocarbons remained in the convective boundary layer, with mixing ratios close to zero ppb in the entrainment zone above the mixed layer (Fig. 2b and c). Isoprene mixing ratios in the ABL exhibited a high sensitivity to variations in  $Z_i$  (Wei et al., 2018), so that even small perturbations in the dynamics of the convective boundary layer considerably impacted the vertical distribution and mixing ratios of isoprene and monoterpenes. While nearly constant  $\theta_{\nu}$  prevailed in the well mixed boundary layer above the canopy (Fig. 2a), isoprene (Iso, Fig. 2b) and monoterpene (Mon, Fig. 2c) levels revealed strong vertical gradients in response to the source strength of the gases in the canopy, and the ensuing turbulent

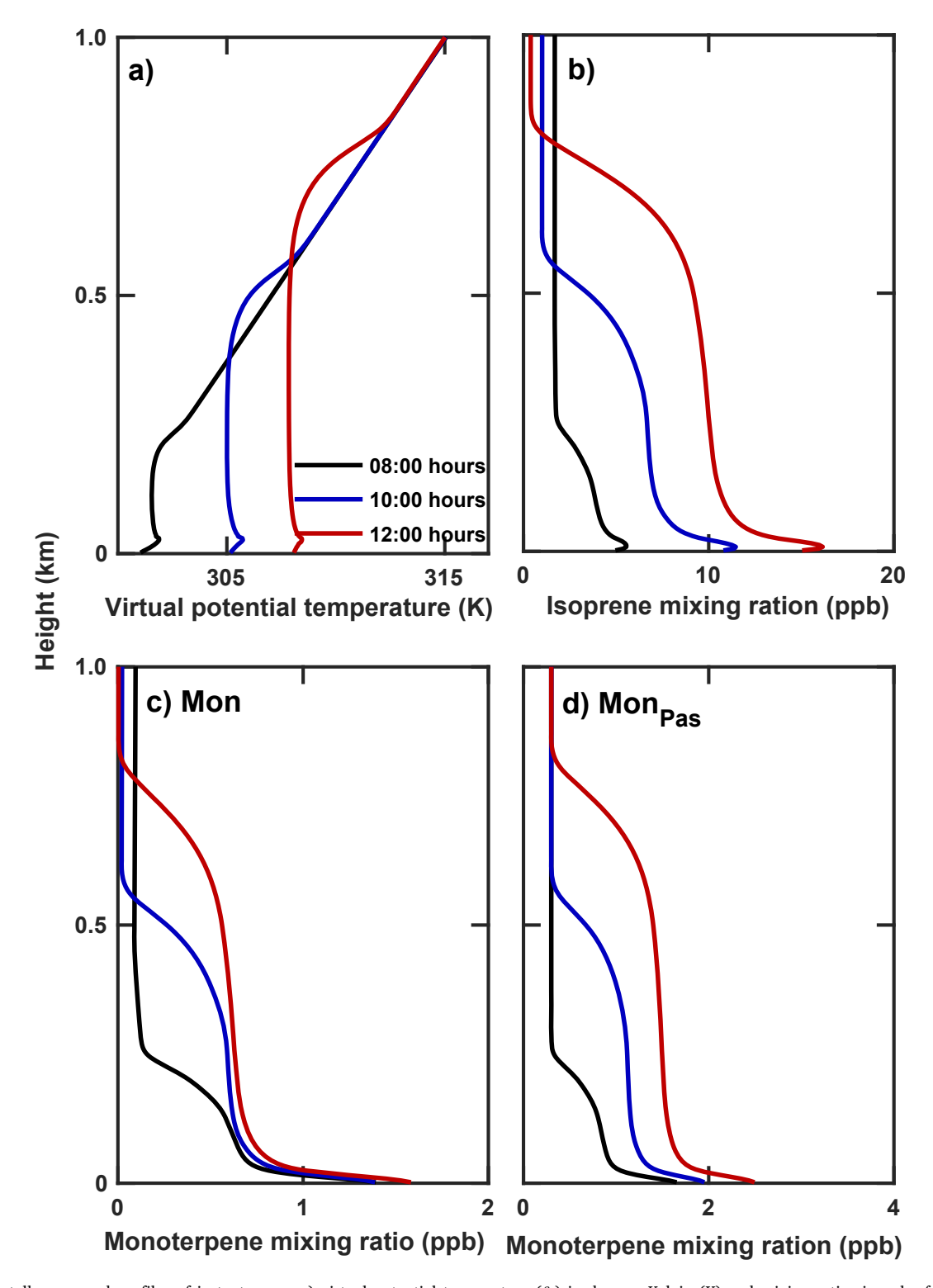


Fig. 2. Horizontally averaged profiles of instantaneous a) virtual potential temperature ( $\theta_{\nu}$ ) in degrees Kelvin (K) and mixing ratios in ppb of b) isoprene, c) monoterpenes (Mon), and d) passive monoterpenes (Mon) at 8:00 (black), 10:00 (blue), and 12:00 h (red) on September 14, 2014. (For interpretation of the references to colour in this figure legend, the reader is referred to the Web version of this article.)

transport and air chemistry. The cases of *Iso* and *Mon* exhibited greatest gas gradients near the forest canopy and the magnitude of gradients increased with height in the upper ABL in response to the gas transport to the free atmosphere and the downward transfer of air parcels nearly devoid of isoprene and monoterpenes from aloft to the top of the mixed layer. Within the mixed layer, the *Iso* and *Mon* cases showed relatively invariant gas mixing ratios with altitude due to the effective

atmospheric turbulent transport. The appreciable differences estimated between the vertical distribution of Mon and  $Mon_{Pas}$  (Fig. 2d) near the forest canopy resulted due to the higher reactivity associated with the Mon case.

Simulated ambient levels of isoprene, monoterpenes, and  $O_3$  were contrasted with observations to ascertain the fidelity of LES outputs. At the canopy top ( $h_c$ ), during 6:00 to 9:00 h temporal patterns of simulated

isoprene (Fig. 3a) closely matched observations. Thereafter, estimated levels of isoprene progressively diverged from observations and reached maximum discrepancies around 12:00 h, leading to approximately 30% higher isoprene mixing ratios than observations. Modeled monoterperpene mixing ratios overestimated the observations (Figure 3b). Differences between simulated and observed monotepene levels steadily increased as simulations proceeded, reaching nearly 35% higher monoterpenes mixing ratios than observations (Figures 3b). Previous studies (Alves et al., 2016) also found greater estimated monoterpene mixing ratios than observations, with higher mixing ratios of total monoterpenes estimated during daytime in response to the light-dependent emissions (Rinne et al., 2002; Kuhn et al., 2002; Jardine et al., 2015a), and the likely inadequate representation the actual light-dependent behavior of monoterpene emissions in low light conditions in the morning hours. As demonstrated in previous studies (Kuhn et al., 2007; Alves et al., 2016), emissions of isoprene and monoterpenes were likely overestimated in response to variations in the basal emissions throughout the canopy environment. Also, mixing ratios of isoprene and monoterpenes were sensitive to variations in the values of Z<sub>i</sub> (Wei et al., 2018) so that underestimation of simulated mixing-layer heights in the LES may be responsible for the overestimation of above canopy isoprene and monoterpene mixing ratio. Simulated temporal variations of  $O_3$  mixing ratio at the canopy top closely matched observations (Figure 3c), with LES results underpredicting  $O_3$  by an average of 5%. At z  $h_c^{-1}=1.14$ , the  $O_3$  levels varied from 12 to 24 ppb over the course of the simulation period (Figure 3c). Once the influences of chemical reactions were integrated for the full canopy, the *Iso, Mon*, and *Pin* scenarios produced similar patterns in ambient gas levels at the canopy top (Fig. 3).

#### 3.2. Processes controlling canopy budgets of isoprene and monoterpenes

Emissions and turbulent transport dominated the processes controlling the isoprene budget in the rainforest canopy. At midday, isoprene emissions contributed to 80 ppbv  $h^{-1}$  whereas turbulent transport carried 75 ppbv  $h^{-1}$  out of the canopy. On average, surface deposition and air chemistry accounted for 1–2% and < 5% of the total isoprene budget destroyed in the canopy (Fig. 4a), respectively. The condensed photochemical mechanism (Table S1) employed to investigate chemical reactions in the canopy did not consider the influences of HO recycling associated with isoprene oxidation (Taraborrelli et al., 2012; Fuchs et al., 2013). The small chemical loss resulted because most of the

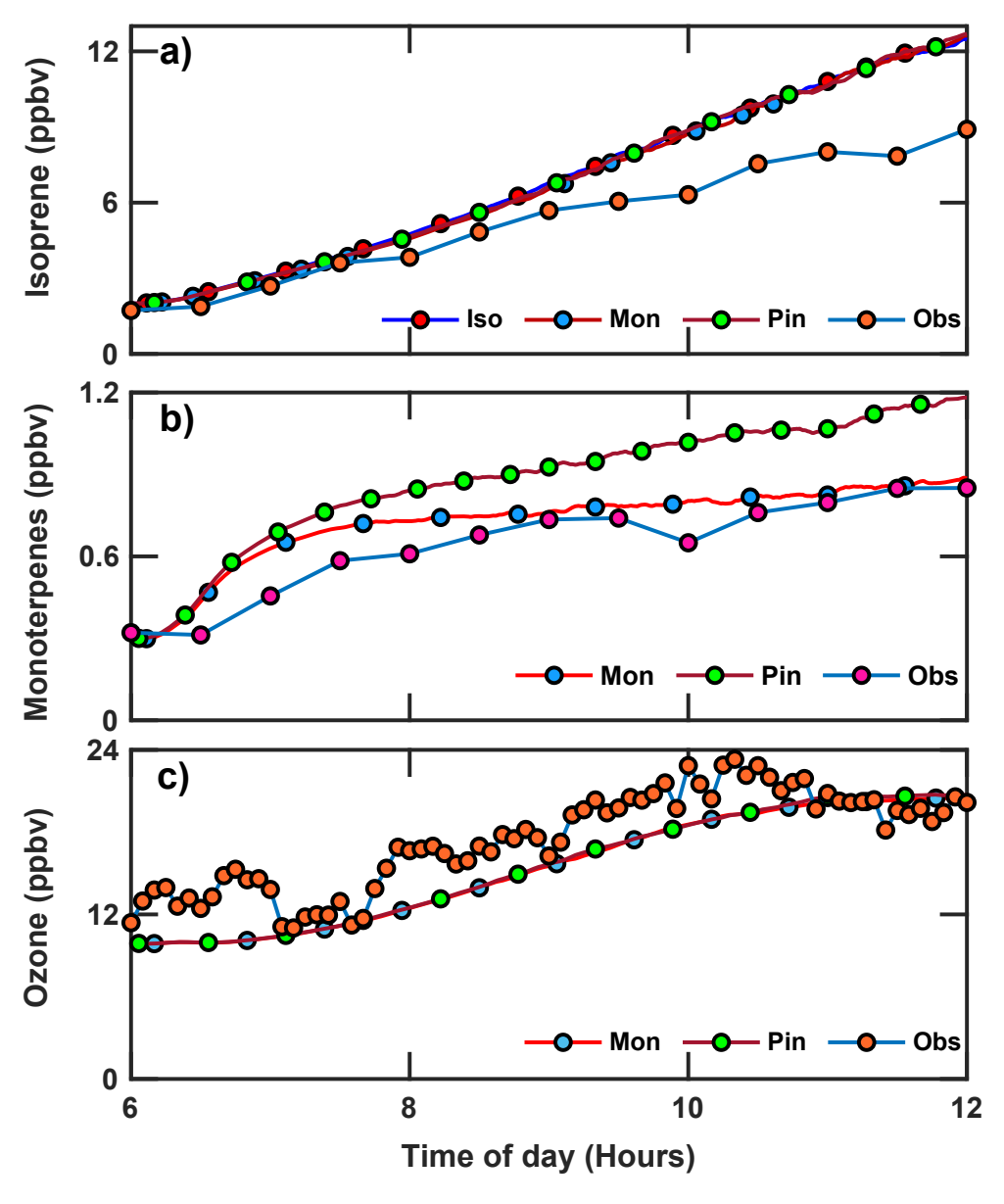


Fig. 3. Simulated and observed gas mixing ratios in ppb at  $\mathrm{zh}_c^{-1}=1.14$  of a) isoprene (the *Iso* case indicates only isoprene chemistry, *Mon* means that the chemistry of monoterpenes was added to the isoprene chemistry, *Pin* means the chemistry of  $\alpha$ -pinene was added to the isoprene chemistry), b) monoterpenes (*Mon* indicates that the chemistry of monoterpenes was combined with isoprene chemistry, *Pin* means the chemistry of  $\alpha$ -pinene was added to the isoprene chemistry), and c) ozone for cases *Iso*, *Mon*, and *Pin* on September 14, 2014. Shaded circles represent select times when data are plotted.

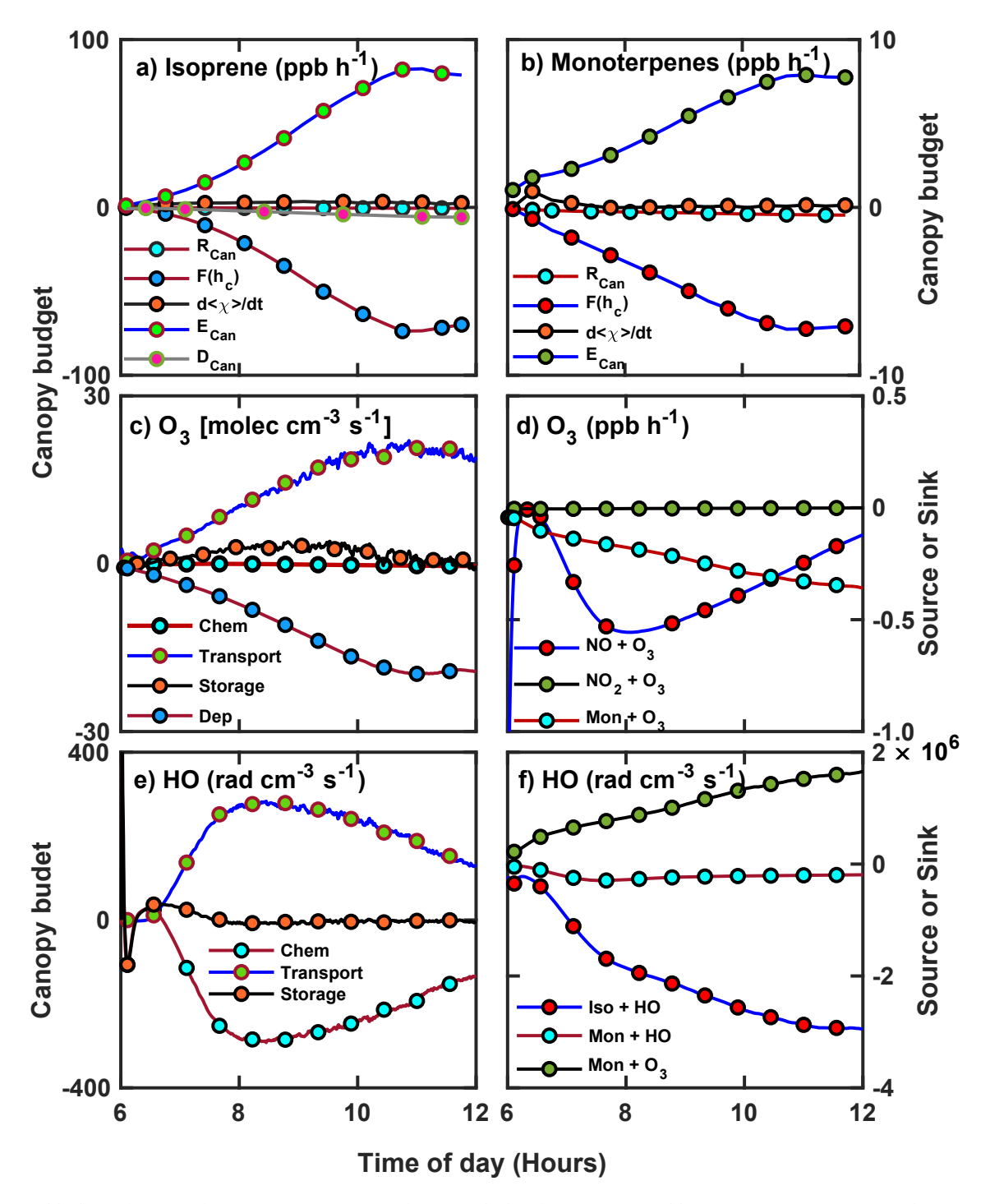


Fig. 4. Computed budgets of gases at the canopy top. a) Terms in the canopy budget for a) isoprene and b) monoterpenes (Mon case). Budget terms include air chemistry ( $R_{Can}$ ), flux across canopy top ( $F(h_c)$ ), change in gas storage ( $d < \chi > /dt$ ), canopy emission ( $E_{Can}$ ), and surface deposition ( $D_{Can}$ ), which was calculated as the residual of the other terms. Positive values indicate accumulation in the control volume. c) Terms (air chemistry, transport, storage, and surface deposition) of the ozone canopy budget. d) Rates of ozone destruction due to reactions with nitric oxide ( $NO_c$ ), nitrogen dioxide ( $NO_c$ ), and mmonoterpenes ( $NO_c$ ) are the hydroxyl radical budget. f) Rates of hydroxyl radical destruction or formation due to reactions with isoprene, monoterpenes, and ozonolysis of monoterpenes on September 14, 2014. Shaded circles represent select times when data are plotted.

isoprene was emitted in the forest crown (Fig. 1e) where air turbulence became strongest and median air parcel residence times varied from seconds to 10 min (Gerken et al., 2017). Such time scales were much shorter than the isoprene lifetime of about 1.0 h due to the HO reaction. In addition, limited isoprene emissions occurred in the lower region of the forest canopy (Fig. 1e) where actinic irradiance (Moon et al., 2020) and oxidant levels (Freire et al., 2017) ordinarily remained low to drive isoprene chemical reactions. Similar patterns in the budget terms

prevailed for monoterpenes, with emissions and turbulent transport contributing with 8.5 and 7.5 ppbv h $^{-1}$  (Fig. 4b), respectively. For the *Mon* case, in-canopy oxidation removed approximately 5–10% of emitted monoterpenes. In contrast, for the *Pin* scenario, reactions destroyed 3–5% of emitted gases due to the lower reactivity (for  $\alpha$ -pinene) assumed in the photochemical mechanism (see Fig. S5 of the Supplement). Compared to isoprene, the greater chemical loss occurred because emissions of monoterpenes prevailed throughout the canopy

(Fig. 1f) where air parcels remained long enough to allow chemical reactions to occur and generate HO, thereby producing a positive feedback loop to augment chemical reactions involving HO in the full canopy volume. Previous studies (Makar et al., 1999; Stroud et al., 2005; Fuentes et al., 2007) reported similar results for monoterpenes in temperate forests. Hence, one conclusion is that chemical processing in tropical, dense forests consumes appreciable amounts of monotertpenes

(Figure 4b) and needs to be considered in numerical models designed to determine BVOC budgets.

Ozone and HO dominated the oxidation of monoterpenes whereas HO controlled the isoprene chemistry in the forest canopy. Based on the individual terms of the mass budget relationship (6), turbulent transport and surface deposition accounted for 38% and 35% of the O<sub>3</sub> budget (Fig. 4c), respectively. These results agreed with earlier findings (Freire

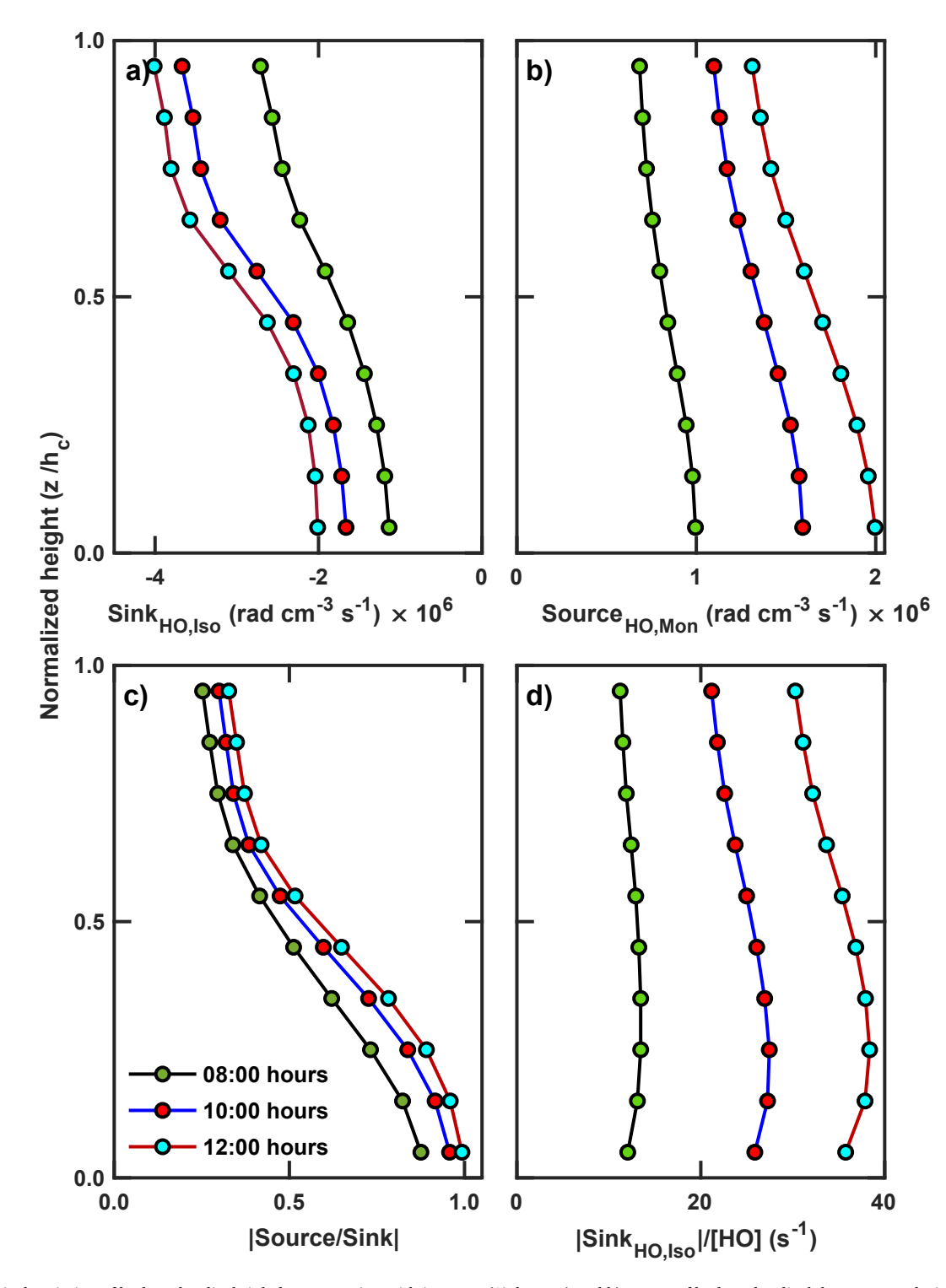


Fig. 5. a) Vertical variation of hydroxyl radical sink due to reaction with isoprene ( $Sink_{HO,Isop}$ ) and b) source of hydroxyl radical due to rozonolysis of monoterpenes ( $Source_{HO,Mon}$ ). c) Comparison of source and sink strength of hydroxyl radical as a function of canopy depth. d) The absolute ratio of hydroxyl radical sink due to reaction with isoprene to average ambient hydroxyl radical concentration as a function of canopy depth for 08:00, 10:00, and 12:00 h on September 14, 2014. Shaded circles represent select heights where data are plotted.

et al., 2017). On average, the  $O_3$  sink due to chemical reactions in the canopy represented 5% of the canopy budget. The small chemical  $O_3$  sink (Fig. 4c) resulted largely in response to the low NO levels (< 0.5 ppb) and relatively slow rate of  $O_3$  reaction with isoprene ( $k_{O_3,\text{lso}} = 1.30 \times 10^{-17} \, \text{cm}^3 \, \text{molec}^{-1} \, \text{s}^{-1}$ ), which was the dominant hydrocarbon in the forest canopy (Fuentes et al., 2016). The  $O_3$  plus NO reaction only consumed 0.5 ppb h<sup>-1</sup> whereas reactions with monoterpenes removed  $O_3$  molecules at the rate of 0.4 ppb h<sup>-1</sup> (Fig. 4d). Trace NO<sub>2</sub> levels (< 0.1 ppb) prevailed in the forest canopy. As a result, the sink for  $O_3$  due to reaction with NO<sub>2</sub> reached nearly 0 ppb h<sup>-1</sup> (Fig. 4d). Sesquiterpenes were not considered in the photochemical mechanism, but such gases could represent a significant sink for  $O_3$  within the canopy due to their rapid ozonelysis (Jardine et al., 2011, 2015a) whose reactivity value could be as high as  $k_{O_3,\text{Caryo}} = 1.16 \times 10^{-14} \, \text{cm}^3 \, \text{molec}^{-1} \, \text{s}^{-1}$  for the  $\beta$  – caryophyllene ( $C_{15}H_{24}$ ) molecule.

In the case of HO, chemical reaction rates nearly balanced the net turbulent (upward and downward) transport, each budget term amounting to absolute values of approximately 350 radicals cm $^{-3}$  s $^{-1}$ . As expected, the storage term remained close to zero radicals cm<sup>-3</sup> s<sup>-1</sup> in response to the rapid formation and destruction of HO (Fig. 4 e). Individual reactions revealed the salient HO sinks and sources (contributions of select individual reactions were estimated indirectly from the reaction constants and modeled concentrations). For example, the reaction rate of monoterpenes with HO (R28) produced 1.8  $\times$   $\bar{10}^6$  radicals  $\text{cm}^{-3}~\text{s}^{-1}$ whereas the reaction rate of isoprene with HO (R9) consumed  $3.0 \times 10^6$ radicals cm<sup>-3</sup> s<sup>-1</sup> (Fig. 4 f). The HO source from the ozonolysis of monoterpenes in the rainforest closely agreed with previous estimates of 10<sup>6</sup> radicals cm<sup>-3</sup> s<sup>-1</sup> (Gerken et al., 2016). The HO formation or consumption rates occurred while averaged mixing ratios of monoterpenes and isoprene reached 1 and 10 ppb, respectively, with prevailing NO levels of < 0.5 ppb in the forest canopy. The abundance of isoprene dominated the HO sink in the upper canopy. Due to the high reactivity of monoterpenes with O<sub>3</sub>, the HO source from the reaction of monoterpenes with O<sub>3</sub> (R29) greatly exceeded the HO sink from the reaction of monoterpenes with HO (R28). In the forest canopy, O<sub>3</sub> and monoterpenes had much greater mixing ratios than HO levels and also had greater lifetimes. Therefore, the magnitude of the estimated HO source became less affected by competing reactions than the HO sink from isoprene reactions. This finding highlights the crucial role of monoterpenes in maintaining a photochemically active forest environment through the generation of HO.

## 3.3. Vertical variability of HO source and sinks in the forest canopy

Source and sink of HO resulting from the oxidation of isoprene and monoterpenes exhibited strong vertical variations in the forest canopy. The LES results showed that HO concentrations associated with isoprene reaction (R9) increased (i.e., became more negative) with time of day and decreased with canopy depth (Fig. 5 a). Maximum HO consumption occurred around 12:00 h when the destruction rate reached  $-4.0 \times 10^6$ radicals cm  $^{-3}$ s $^{-1}$  in the upper (z/h $_c$  > 0.85) canopy. At the canopy depth of  $z/h_c = 0.25$ , the HO destruction rate was 50% lower than the values determined in the forest crown in response to the reduced actinic irradiance flux due to canopy shading, which reduced photochemical production of HO (R1 + R2), and limited isoprene emissions. In contrast, the HO formation rate resulting from oxidation of monoterpenes (Mon, Pin) increased with time of day and canopy depth (Fig. 5 b). Despite the comparatively low ambient  $O_3$  levels in Amazonia ( $\overline{[O_3]} \sim 10$  ppb) during the wet season (Dias-Junior et al., 2017), the ozonelysis of monoterpenes (R29) yielded maximum HO formation rates ranging from  $+2.0 \times 10^6$  radicals cm<sup>-3</sup> s<sup>-1</sup> in the lower canopy to  $+1.3 \times 10^6$ radicals cm<sup>-3</sup> s<sup>-1</sup> in the forest crown around 12:00 h. Compared to the Pin scenario, the Mon case contributed to greater HO yield (see the Supplement) due to the higher O3 reactivity for the assumed average monoterpene ( $k_{O_{3,Mono}} = 1.82 \times 10^{-16}$  versus  $k_{O_{3,Pin}} = 8.09 \times 10^{-16}$ 

 $10^{-17} \,\mathrm{cm^3 \,molec^{-1} \,s^{-1}}$ ). The HO formation rates (Fig. 5 a, b) were computed while the range of NO levels prevailed < 0.5 ppb. However, as confirmed by previous studies (Rohrer et al., 2014; Vilà-Guerau de Arellano et al., 2011; Wei et al., 2018), HO yields strongly depend on NOx concentrations. As revealed by the fraction of HO production from oxidation of monoterpenes (R28, R29) to HO consumption by isoprene (R9), sources and sinks of HO remained closely in balance at canopy depths  $z/h_c < 0.25$  (Fig. 5 c). In addition, the absolute ratio of HO destruction rate (involving the isoprene reaction) to the simulated HO concentration ( $\left|Sink_{HO_{Iso}}\right|/\left[HO\right]$ ), which was a measured of HO reactivity in the canopy, exhibited minor variations with canopy depth. The LES-derived HO reactivity values for isoprene varied from 10 s<sup>-1</sup> at 08:00 h to 40 s<sup>-1</sup> at 12:00 h. The computed reactivity values were similar to the daytime quantities of  $10-30 \text{ s}^{-1}$  observed in an Amazonian rainforest during the dry season (Nölscher et al., 2016a,b). Overall, the oxidation of monoterpenes in the lower forest canopy ( $z/h_c < 0.25$ ) generated enough HO to balance the HO needed to drive the isoprene reaction (Fig. 5). Because the Amazon rainforest emits a plethora of reactive sesquiterpenes (not considered in this study) and monoterpenes (Jardine et al., 2015a), the HO production from oxidation of emitted hydrocarbons can be greater than the values (Fig. 5) reported in this study. Additionally, HO yields from ozonelysis of monoterpenes and sesquiterpenes can be expected to greatly vary in response to increases in NOx levels associated with biomass burning and/or regional air pollution (Wei et al., 2019). In the central Amazon, sesquiterpenes (such as  $\beta$ -caryophyllene,  $\alpha$ -humulene,  $\alpha$ -copaene) can reach mixing ratios of 0.5 ppb in the crown of the rainforest (Jardine et al., 2011).

#### 4. Summary and conclusions

Based on the three posed research questions, several conclusions were derived. First, emissions, turbulent transport, surface deposition, and chemical reactions governed temporal and spatial patterns of isoprene and monoterpenes in and above the rainforest. Despite sufficient active biomass distributed throughout the canopy volume, approximately 85% of isoprene emissions came from the upper  $(z/h_c)$ 0.40) canopy. Maximum isoprene emission density reached 400  $\mu g \ m^{-3}$  $h^{-1}$  at  $z/h_c \approx 0.60$  around noontime. In part, the greater emissions in the forest crown occurred because the high leaf area density in the upper canopy intercepted most of the incoming photosynthetically active radiation needed to promote isoprene emissions. In contrast, emissions of monoterpenes occurred throughout the forest canopy in response to the suitable conditions (e.g., temperature) to drive emissions. The greatest emission density of monoterpenes was 75  $\mu g~m^{-3}~h^{-1}$  at  $z/h_c \approx 0.60$ around noontime. The unusually high emission densities gave rise to maximum ambient levels of isoprene and monoterpenes of 8 and 0.8 ppb, respectively, at  $z/h_c = 1.14$ . Mixing ratios of isoprene and monoterpenes remained effectively dispersed in the mixed layer but rapidly decreased with altitude in the upper region of the convective boundary layer, attaining mixing ratio values close to zero ppb just above the entrainment zone.

Second, chemical reactions and surface deposition destroyed some isoprene and monoterpenes in the forest canopy. Under the influences of observed ozone (<25 ppb) and nitric oxide (<0.5 ppb) levels, isoprene destruction due to the chemical reactions amounted to <5% of the canopy emissions. The reaction with the hydroxyl radical dominated the chemical sink of isoprene in the canopy. The small chemical loss resulted because most of the emitted isoprene occurred in the upper canopy where air parcel residence times were substantially shorter than the isoprene lifetime. In addition, while substantial isoprene levels persisted in the forest canopy, the low ozone (directly) and nitric oxide (indirectly) levels limited the isoprene chemical sink. In the case of monoterpenes, chemical reactions destroyed approximately 10% of the total canopy emissions. The ozonelysis of monoterpenes became the dominant chemical sink in the canopy. Because emissions of monoterpenes

took place throughout the canopy and air parcels in the lower canopy had longer residence times, the molecules had greater likelihood to partake in chemical reactions before the gases were exported out of the forest canopy.

Third, concomitant and copious emissions of isoprene and monoterpenes within the tropical forest canopy mixed and interacted with ozone and hydroxyl radical to create a unique chemical environment. While both ozone and hydroxyl radical contributed to the oxidation of isoprene and monoterpenes, their role for in-canopy air chemistry was fundamentally different. Ozone was principally carried from aloft into the canopy through turbulent transport whereas hydroxyl radical was continuously produced, destroyed, and recycled in the rainforest canopy. Decreasing actinic fluxes due to shading in the dense canopy reduced light-dependent hydroxyl radical formation rates in the lower air canopy layers. At the same time, the ozonelysis became the most important chemical sink of monoterpenes and contributed to the formation of hydroxyl radical whose yield reached  $\approx 2 \times$  $10^6 \, \mathrm{radicals} \, \mathrm{cm}^{-3} \, \mathrm{s}^{-1}$ . Therefore, in dense forest canopies with co–located emissions of isoprene and monoterpenes, the oxidation of hydrocarbon molecules can produce sufficient hydroxyl radical levels to maintain a photochemically active environment. The degree of photochemical activity in the canopy would substantially depend on the levels of both ozone and nitrogen oxides, and reactivity of emitted hydrocarbon molecules.

#### CRediT authorship contribution statement

Jose D. Fuentes: Conceptualization, Methodology, and, writing of article text. Tobias Gerken: Conceptualization, Methodology, and, writing of article text. Marcelo Chamecki: Conceptualization, Methodology, and writing of article text. Paul Stoy: contributed with field data acquisition and proofread the manuscript. Livia Freire: Data acquisition and interpretation, contributed with field data acquisition and proofread the manuscript. Jesus Ruiz-Plancarte: Data acquisition and interpretation, contributed with field data acquisition and proofread the manuscript.

#### Declaration of competing interest

The authors declare that they have no known competing financial interests or personal relationships that could have appeared to influence the work reported in this paper.

#### Acknowledgments

The authors thank G. Katul for comments and suggestions. The U.S. Department of Energy supported the field studies as part of the GoAmazon 2014/5 project (grant SC0011075). Fundação de Amparo à Pesquisa do Estado de São Paulo (FAPESP) and Fundação de Amparo à Pesquisa do Estado do Amazonas (FAPEAM) funded the Brazilian component of the field studies. The Large scale Biosphere-Atmosphere Experiment in Amazonia (LBA) provided logistic support and made the flux tower and housing unit available to complete the field studies. We thank the support from the LBA central office that operated at INPA. We acknowledge logistical support from the ARM Climate Research Facility. JDF acknowledges support from the National Oceanic and Atmospheric Administration, Educational Partnership Program, U.S. Department of Commerce, under Agreement No. NA16SEC4810006-NCAS-M and the National Science Foundation (Award 2000403). The data needed for reproducing the figures are available from the authors upon request. We thank an anonymous reviewer who provided excellent comments to improve the original manuscript.

#### Appendix A. Supplementary data

Supplementary data to this article can be found online at https://doi.org/10.1016/j.atmosenv.2022.119094.

#### References

- Alves, E.G., Jardine, K., Tota, J., Jardine, A., Yānez-Serrano, A.M., Karl, T., Tavares, J., Nelson, B., Gu, D., Stavrakou, T., et al., 2016. Seasonality of isoprenoid emissions from a primary rainforest in central Amazonia. Atmos. Chem. Phys. 16, 3903–3925.
- Arneth, A., Schurgers, G., Lathiere, J., Duhl, T., Beerling, D., Hewitt, C., Martin, M., Guenther, A., 2011. Global terrestrial isoprene emission models: sensitivity to variability in climate and vegetation. Atmos. Chem. Phys. 11, 8037–8052.
- Aschmann, S.M., Arey, J., Atkinson, R., 2002. OH radical formation from the gas-phase reactions of O<sub>3</sub> with a series of terpenes. Atmos. Environ. 36, 4347–4355.
- Atkinson, R., 2000. Atmospheric chemistry of VOCs and NO<sub>x</sub>. Atmos. Environ. 34, 2063–2101
- Atkinson, R., Aschmann, S.M., Arey, J., Shorees, B., 1992. Formation of OH radicals in the gas phase reactions of O<sub>3</sub> with a series of terpenes. J. Geophys. Res. Atmos. 97, 6065–6073.
- Barr, J., Fuentes, J., Bottenheim, J., 2003. Radiative forcing of phytogenic aerosols. J. Geophys. Res. Atmos. 108.
- Bates, K.H., Jacob, D.J., 2019. A new model mechanism for atmospheric oxidation of isoprene: global effects on oxidants, nitrogen oxides, organic products, and secondary organic aerosol. Atmos. Chem. Phys. 19, 9613–9640.
- Bou-Zeid, E., Meneveau, C., Parlange, M.B., 2004. Large-eddy simulation of neutral atmospheric boundary layer flow over heterogeneous surfaces: blending height and effective surface roughness. Water Resour. Res. 40, W02505. https://doi.org/ 10.1029/2003WR002475
- Chamecki, M., Meneveau, C., Parlange, M.B., 2008. A hybrid spectral/finite-volume algorithm for Large-Eddy Simulation of scalars in the atmospheric boundary layer. Boundary-Layer Meteorol. 128, 473–484. https://doi.org/10.1007/s10546-008-9302-1.
- Chamecki, M., Meneveau, C., Parlange, M.B., 2009. Large eddy simulation of pollen transport in the atmospheric boundary layer. J. Aerosol Sci. 40, 241–255. https:// doi.org/10.1016/j.jaerosci.2008.11.004. URL: http://www.sciencedirect.com/sci ence/article/pii/S0021850208002024.
- Dai, Y., Dickinson, R.E., Wang, Y.P., 2004. A two-big-leaf model for canopy temperature, photosynthesis, and stomatal conductance. J. Clim. 17, 2281–2299. https://doi.org/ 10.1175/1520-0442(2004)017<2281:ATMFCT>2.0.CO:2.
- Dias-Junior, C.Q., Dias, N.L., Fuentes, J.D., Chamecki, M., 2017. Convective storms and non-classical low-level jets during high ozone level episodes in the Amazon region: an ARM/GOAMAZON case study. Atmos. Environ. 155, 199–209.
- Edburg, S.L., Stock, D., Lamb, B.K., Patton, E.G., 2011. The effect of the vertical source distribution on scalar statistics within and above a forest canopy. Boundary-Layer Meteorol. 142, 365–382. https://doi.org/10.1007/s10546-011-9686-1.
- Edwards, P., Evans, M., Furneaux, K., Hopkins, J., Ingham, T., Jones, C., Lee, J., Lewis, A., Moller, S., Stone, D., et al., 2013. OH reactivity in a South East Asian tropical rainforest during the oxidant and particle photochemical processes (OP3) project. Atmos. Chem. Phys. 13, 9497–9514.
- Emmons, L.K., Walters, S., Hess, P.G., Lamarque, J.F., Pfister, G.G., Fillmore, D., Granier, C., Guenther, A., Kinnison, D., Laepple, T., Orlando, J., Tie, X., Tyndall, G., Wiedinmyer, C., Baughcum, S.L., Kloster, S., 2010. Description and evaluation of the model for ozone and related chemical tracers, version 4 (MOZART-4). Geosci. Model Dev 3, 43–67. https://doi.org/10.5194/gmd-3-43-2010. URL: http://www.geosci-model-dev.net/3/43/2010/.
- Finnigan, J., 2000. Turbulence in plant canopies. Annu. Rev. Fluid Mech. 32, 519–571.
- Fisch, G., Tota, J., Machado, L.a.T., Dias, M.A.F.S., Lyra, R.F.d.F., Nobre, C.A., Dolman, A.J., Gash, J.H.C., 2004. The convective boundary layer over pasture and forest in Amazonia. Theor. Appl. Climatol. 78, 47–59. https://doi.org/10.1007/s00704-004-0043-x.
- Fitzjarrald, D.R., Moore, K.E., 1990. Mechanisms of nocturnal exchange between the rain forest and the atmosphere. J. Geophys. Res. Atmos. 95, 16839–16850.
- Fitzjarrald, D.R., Moore, K.E., Cabral, O.M., Scolar, J., Manzi, A.O., de Abreu Sá, L.D., 1990. Daytime turbulent exchange between the Amazon forest and the atmosphere. J. Geophys. Res. Atmos. 95, 16825–16838.
- Foken, T., 2006. 50 years of the Monin–Obukhov similarity theory. Boundary-Layer Meteorol. 119, 431–447.
- Freire, L., Gerken, T., Ruiz-Plancarte, J., Wei, D., Fuentes, J., Katul, G., Dias, N., Acevedo, O., Chamecki, M., 2017. Turbulent mixing and removal of ozone within an Amazon rainforest canopy. J. Geophys. Res. Atmos. 122, 2791–2811.
- Fuchs, H., Hofzumahaus, A., Rohrer, F., Bohn, B., Brauers, T., Dorn, H., Häseler, R., Holland, F., Kaminski, M., Li, X., et al., 2013. Experimental evidence for efficient hydroxyl radical regeneration in isoprene oxidation. Nat. Geosci. 6, 1023–1026.
- Fuentes, J., Wang, D., Gu, L., 1999. Seasonal variations in isoprene emissions from a boreal aspen forest. J. Appl. Meteorol. 38, 855–869.
- Fuentes, J.D., Chamecki, M., Nascimento dos Santos, R.M., Von Randow, C., Stoy, P.C., Katul, G., Fitzjarrald, D., Manzi, A., Gerken, T., Trowbridge, A., et al., 2016. Linking meteorology, turbulence, and air chemistry in the Amazon rain forest. Bull. Am. Meteorol. Soc. 97, 2329–2342.
- Fuentes, J.D., Lerdau, M., Atkinson, R., Baldocchi, D., Bottenheim, J., Ciccioli, P., Lamb, B., Geron, C., Gu, L., Guenther, A., et al., 2000. Biogenic hydrocarbons in the atmospheric boundary layer: a review. Bull. Am. Meteorol. Soc. 81, 1537–1575.

- Fuentes, J.D., Wang, D., Bowling, D.R., Potosnak, M., Monson, R.K., Goliff, W.S., Stockwell, W.R., 2007. Biogenic hydrocarbon chemistry within and above a mixed deciduous forest. J. Atmos. Chem. 56, 165–185.
- Gaskell, P.H., Lau, A.K.C., 1988. Curvature-compensated convective transport: SMART, A new boundedness-preserving transport algorithm. Int. J. Numer. Methods Fluid. 8, 617–641. https://doi.org/10.1002/fld.1650080602.
- Geiger, H., Barnes, I., Bejan, I., Benter, T., Spittler, M., 2003. The tropospheric degradation of isoprene: an updated module for the regional atmospheric chemistry mechanism. Atmos. Environ. 37, 1503–1519. https://doi.org/10.1016/S1352-2310 (02)01047-6. URL: http://www.sciencedirect.com/science/article/pii/S1352231 002010476.
- Gerken, T., Chamecki, M., Fuentes, J.D., 2017. Air-parcel residence times within forest canopies. Boundary-Layer Meteorol. 165, 29–54.
- Gerken, T., Wei, D., Chase, R.J., Fuentes, J.D., Schumacher, C., Machado, L.A., Andreoli, R.V., Chamecki, M., de Souza, R.A.F., Freire, L.S., et al., 2016. Downward transport of ozone rich air and implications for atmospheric chemistry in the Amazon rainforest. Atmos. Environ. 124, 64–76.
- Gordon, M., Vlasenko, A., Staebler, R.M., Stroud, C., Makar, P.A., Liggio, J., Li, S.M., Brown, S., 2014. Uptake and emission of VOCs near ground level below a mixed forest at Borden, Ontario. Atmos. Chem. Phys. 14, 9087–9097. https://doi.org/ 10.5194/acp-14-9087-2014. URL: http://www.atmos-chem-phys.net/14/9 087/2014/.
- Gu, L., 1999. Modeling Biophysical Exchanges and Micro-meteorology in Soil-Vegetation-Atmosphere Continuum: Results from a Two-Story Boreal Aspen Forest. PhD Dissertation. University of Virginia, Charlottesville, Virginia, United States.
- Guenther, A., Karl, T., Harley, P., Wiedinmyer, C., Palmer, P.I., Geron, C., 2006.
  Estimates of global terrestrial isoprene emissions using MEGAN (model of emissions of gases and aerosols from Nature). Atmos. Chem. Phys. 6, 3181–3210. https://doi.org/10.5194/acp-6-3181-2006. URL: http://www.atmos-chem-phys.net/6/3
  181/2006/
- Guenther, A.B., Jiang, X., Heald, C.L., Sakulyanontvittaya, T., Duhl, T., Emmons, L.K., Wang, X., 2012. The Model of Emissions of Gases and Aerosols from Nature version 2.1 (MEGAN2.1): an extended and updated framework for modeling biogenic emissions. Geosci. Model Dev. (GMD) 5, 1471–1492. https://doi.org/10.5194/gmd-5-1471-2012. URL: http://www.geosci-model-dev.net/5/1471/2012/gmd-5-1471-2012.html.
- Herrmann, F., Winterhalter, R., Moortgat, G.K., Williams, J., 2010. Hydroxyl radical (OH) yields from the ozonolysis of both double bonds for five monoterpenes. Atmos. Environ. 44, 3458–3464.
- Heus, T., van Heerwaarden, C.C., Jonker, H.J.J., Pier Siebesma, A., Axelsen, S., van den Dries, K., Geoffroy, O., Moene, A.F., Pino, D., de Roode, S.R., Vilà-Guerau de Arellano, J., 2010. Formulation of the Dutch atmospheric large-eddy simulation (DALES) and overview of its applications. Geosci. Model Dev. (GMD) 3, 415–444. https://doi.org/10.5194/gmd-3-415-2010. URL: http://www.geosci-model-dev.net/3/415/2010/.
- Jardine, A.B., Jardine, K.J., Fuentes, J.D., Martin, S.T., Martins, G., Durgante, F., Carneiro, V., Higuchi, N., Manzi, A.O., Chambers, J.Q., 2015a. Highly reactive light-dependent monoterpenes in the Amazon. Geophys. Res. Lett. 42, 1576–1583.
- Jardine, K.J., Chambers, J.Q., Holm, J., Jardine, A.B., Fontes, C.G., Zorzanelli, R.F., Meyers, K.T., De Souza, V.F., Garcia, S., Gimenez, B.O., et al., 2015b. Green leaf volatile emissions during high temperature and drought stress in a central Amazon rainforest. Plants 4, 678–690.
- Jardine, K.J., Yañez Serrano, A., Arneth, A., Abrell, L., Jardine, A., Van Haren, J., Artaxo, P., Rizzo, L.V., Ishida, F.Y., Karl, T., et al., 2011. Within-canopy sesquiterpene ozonolysis in Amazonia. J. Geophys. Res. Atmos. 116.
- Karl, T., Guenther, A., Yokelson, R.J., Greenberg, J., Potosnak, M., Blake, D.R., Artaxo, P., 2007. The tropical forest and fire emissions experiment: emission, chemistry, and transport of biogenic volatile organic compounds in the lower atmosphere over Amazonia. J. Geophys. Res. Atmos. 112, D18302. https://doi.org/ 10.1029/2007.JD008539.
- Khan, B., Banzhaf, S., Chan, E.C., Forkel, R., Kanani-Sühring, F., Ketelsen, K., Kurppa, M., Maronga, B., Mauder, M., Raasch, S., et al., 2021. Development of an atmospheric chemistry model coupled to the PALM model system 6.0: implementation and first applications. Geosci. Model Dev. (GMD) 14, 1171–1193.
- Kruijt, B., Malhi, Y., Lloyd, J., Norbre, A., Miranda, A., Pereira, M.G., Culf, A., Grace, J., 2000. Turbulence statistics above and within two Amazon rain forest canopies. Boundary-Layer Meteorol. 94, 297–331.
- Kuhn, U., Andreae, M.O., Ammann, C., Araújo, A., Brancaleoni, E., Ciccioli, P., Dindorf, T., Frattoni, M., Gatti, L.V., Ganzeveld, L., et al., 2007. Isoprene and monoterpene fluxes from central Amazonian rainforest inferred from tower-based and airborne measurements, and implications on the atmospheric chemistry and the local carbon budget. Atmos. Chem. Phys. 7, 2855–2879.
- Kuhn, U., Rottenberger, S., Biesenthal, T., Wolf, A., Schebeske, G., Ciccioli, P., Brancaleoni, E., Frattoni, M., Tavares, T., Kesselmeier, J., 2002. Isoprene and monoterpene emissions of amazonian tree species during the wet season: direct and indirect investigations on controlling environmental functions. J. Geophys. Res. Atmos. 107. LBA–38.
- Lelieveld, J., Butler, T., Crowley, J., Dillon, T., Fischer, H., Ganzeveld, L., Harder, H., Lawrence, M., Martinez, M., Taraborrelli, D., et al., 2008. Atmospheric oxidation capacity sustained by a tropical forest. Nature 452, 737–740.
- Liu, Y., Brito, J., Dorris, M.R., Rivera-Rios, J.C., Seco, R., Bates, K.H., Artaxo, P., Duvoisin, S., Keutsch, F.N., Kim, S., et al., 2016. Isoprene photochemistry over the Amazon rainforest. Proc. Natl. Acad. Sci. Unit. States Am. 113, 6125–6130.
- Liu, Y., Seco, R., Kim, S., Guenther, A.B., Goldstein, A.H., Keutsch, F.N., Springston, S.R., Watson, T.B., Artaxo, P., Souza, R.A., et al., 2018. Isoprene photo-oxidation products

- quantify the effect of pollution on hydroxyl radicals over Amazonia. Sci. Adv. 4, eaar2547
- Makar, P.A., Fuentes, J.D., Wang, D., Staebler, R.M., Wiebe, H.A., 1999. Chemical processing of biogenic hydrocarbons within and above a temperate deciduous forest. J. Geophys. Res. Atmos. 104, 3581–3603.
- Marques Filho, A.d.O., Dallarosa, R.G., Pacheco, V.B., 2005. Radiação solar e distribuição vertical de área foliar em floresta reserva Biológica do Cuieiras ZF2, Manaus. Acta Amazonica 35, 427–436.
- McWilliam, A.L.C., Roberts, J.M., Cabral, O.M.R., Leitao, M.V.B.R., de Costa, A.C.L., Maitelli, G.T., Zamparoni, C.A.G.P., 1993. Leaf area index and above-ground biomass of terra firme rain forest and adjacent clearings in Amazonia. Funct. Ecol. 7, 310–317. https://doi.org/10.2307/2390210.
- Moon, Z., Fuentes, J.D., Staebler, R.M., 2020. Impacts of spectrally resolved irradiance on photolysis frequency calculations within a forest canopy. Agric. For. Meteorol. 291, 108012.
- Nguyen, T.B., Crounse, J.D., Teng, A.P., Clair, J.M.S., Paulot, F., Wolfe, G.M., Wennberg, P.O., 2015. Rapid deposition of oxidized biogenic compounds to a temperate forest. Proc. Natl. Acad. Sci. Unit. States Am. 112, E392–E401.
- Nölscher, A.C., Yañez-Serrano, A.M., Wolff, S., de Araujo, A.C., Lavrič, J.V., Kesselmeier, J., Williams, J., 2016a. Unexpected seasonality in quantity and composition of Amazon rainforest air reactivity. Nat. Commun. 7, 10383. https://doi.org/10.1038/ncomms10383. URL: http://www.nature.com/ncomms/2016/160122/ncomms10383/full/ncomms10383.html.
- Nölscher, A.C., Yáñez-Serrano, A.M., Wolff, S., De Araujo, A.C., Lavrič, J., Kesselmeier, J., Williams, J., 2016b. Unexpected seasonality in quantity and composition of Amazon rainforest air reactivity. Nat. Commun. 7, 1–12.
- Ouwersloot, H.G., de Arellano, J.V.G., van Stratum, B.J.H., Krol, M.C., Lelieveld, J., 2013. Quantifying the transport of subcloud layer reactants by shallow cumulus clouds over the Amazon. J. Geophys. Res. Atmos. 118, 13041–13059. https://doi.org/10.1002/2013JD020431.
- Pan, Y., Chamecki, M., Isard, S.A., 2014. Large-eddy simulation of turbulence and particle dispersion inside the canopy roughness sublayer. J. Fluid Mech. 753, 499–534. https://doi.org/10.1017/jfm.2014.379. URL: http://journals.cambridge. org/article S0022112014003796.
- Patton, E.G., Davis, K.J., Barth, M.C., Sullivan, P.P., 2001. Decaying scalars emitted by a forest canopy: a numerical study. Boundary-Layer Meteorol. 100, 91–129. https:// doi.org/10.1023/A:1019223515444.
- Patton, E.G., Sullivan, P.P., Shaw, R.H., Finnigan, J.J., Weil, J.C., 2016. Atmospheric stability influences on coupled boundary layer and canopy turbulence. J. Atmos. Sci. 73, 1621–1647.
- Peyret, R., Taylor, T.D., 2012. Computational Methods for Fluid Flow. Springer Science & Business Media.
- Pfannerstill, E.Y., Reijrink, N.G., Edtbauer, A., Ringsdorf, A., Zannoni, N., Araújo, A., Ditas, F., Holanda, B.A., Sá, M.O., Tsokankunku, A., et al., 2021. Total OH reactivity over the Amazon rainforest: variability with temperature, wind, rain, altitude, time of day, season, and an overall budget closure. Atmos. Chem. Phys. 21, 6231–6256.
- Pöschl, U., Martin, S., Sinha, B., Chen, Q., Gunthe, S., Huffman, J., Borrmann, S., Farmer, D., Garland, R., Helas, G., et al., 2010. Rainforest aerosols as biogenic nuclei of clouds and precipitation in the Amazon. Science 329, 1513–1516.
- Pöschl, U., Von Kuhlmann, R., Poisson, N., Crutzen, P.J., 2000. Development and intercomparison of condensed isoprene oxidation mechanisms for global atmospheric modeling. J. Atmos. Chem. 37, 29–52.
- Raupach, M.R., Finnigan, J.J., Brunet, Y., 1996. Coherent eddies and turbulence in vegetation canopies: the mixing-layer analogy. In: Boundary-layer Meteorology 25th Anniversary Volume, 1970–1995. Springer, pp. 351–382.
- Rinne, H., Guenther, A., Greenberg, J., Harley, P., 2002. Isoprene and monoterpene fluxes measured above amazonian rainforest and their dependence on light and temperature. Atmos. Environ. 36, 2421–2426.
- Rinne, J., Markkanen, T., Ruuskanen, T., Petäjä, T., Keronen, P., Tang, M., Crowley, J., Rannik, Ü., Vesala, T., 2012. Effect of chemical degradation on fluxes of reactive compounds—a study with a stochastic Lagrangian transport model. Atmos. Chem. Phys. 12, 4843–4854.
- Rohrer, F., Lu, K., Hofzumahaus, A., Bohn, B., Brauers, T., Chang, C.C., Fuchs, H., Häseler, R., Holland, F., Hu, M., et al., 2014. Maximum efficiency in the hydroxylradical-based self-cleansing of the troposphere. Nat. Geosci. 7, 559–563.
- Santos, D.M., Acevedo, O.C., Chamecki, M., Fuentes, J.D., Gerken, T., Stoy, P.C., 2016. Temporal scales of the nocturnal flow within and above a forest canopy in Amazonia. Boundary-Layer Meteorol. 161, 73–98.
- Schwantes, R.H., Emmons, L.K., Orlando, J.J., Barth, M.C., Tyndall, G.S., Hall, S.R., Ullmann, K., Clair, J.M.S., Blake, D.R., Wisthaler, A., et al., 2020. Comprehensive isoprene and terpene gas-phase chemistry improves simulated surface ozone in the southeastern us. Atmos. Chem. Phys. 20, 3739–3776.
- Sellers, P.J., 1985. Canopy reflectance, photosynthesis and transpiration. Int. J. Rem. Sens. 6, 1335–1372. https://doi.org/10.1080/01431168508948283.
- Shaw, R.H., Schumann, U., 1992. Large-eddy simulation of turbulent flow above and within a forest. Boundary-Layer Meteorol. 61, 47–64. https://doi.org/10.1007/ BF02033994.
- Sindelarova, K., Granier, C., Bouarar, I., Guenther, A., Tilmes, S., Stavrakou, T., Müller, J. F., Kuhn, U., Stefani, P., Knorr, W., 2014. Global data set of biogenic VOC emissions calculated by the MEGAN model over the last 30 years. Atmos. Chem. Phys. 14, 9317–9341.
- Strong, C., Fuentes, J., Baldocchi, D., 2004. Reactive hydrocarbon flux footprints during canopy senescence. Agric. For. Meteorol. 127, 159–173.
- Stroud, C., Makar, P., Guenther, A., Geron, C., Turnipseed, A., Nemitz, E., Baker, B., Potosnak, M., Fuentes, J., 2005. Role of canopy–scale photochemistry in modifying

- biogenic-atmosphere exchange of reactive terpene species: results from the CELTIC field study. J. Geophys. Res. Atmos. 110, 1–14.
- Su, L., Patton, E.G., Vilà-Guerau de Arellano, J., Guenther, A.B., Kaser, L., Yuan, B., Xiong, F., Shepson, P.B., Zhang, L., Miller, D.O., Brune, W.H., Baumann, K., Edgerton, E., Weinheimer, A., Misztal, P.K., Park, J.H., Goldstein, A.H., Skog, K.M., Keutsch, F.N., Mak, J.E., 2016. Understanding isoprene photooxidation using observations and modeling over a subtropical forest in the southeastern US. Atmos. Chem. Phys. 16, 7725–7741. https://doi.org/10.5194/acp-16-7725-2016. URL: http://www.atmos-chem-phys.net/16/7725/2016/.
- Taraborrelli, D., Lawrence, M., Crowley, J., Dillon, T., Gromov, S., Groß, C., Vereecken, L., Lelieveld, J., 2012. Hydroxyl radical buffered by isoprene oxidation over tropical forests. Nat. Geosci. 5, 190–193.
- Tota, J., Roy Fitzjarrald, D., da Silva Dias, M.A., 2012. Amazon rainforest exchange of carbon and subcanopy air flow: Manaus LBA site—a complex terrain condition. Sci. World J. 2012.
- Van Stratum, B., Vilà-Guerau de Arellano, J., Ouwersloot, H., Van Den Dries, K., Van Laar, T., Martinez, M., Lelieveld, J., Diesch, J.M., Drewnick, F., Fischer, H., et al., 2012. Case study of the diurnal variability of chemically active species with respect to boundary layer dynamics during domino. Atmos. Chem. Phys. 12, 5329–5341.
- Verwer, J., Simpson, D., 1995. Explicit methods for stiff ODEs from atmospheric chemistry. Appl. Numer. Math. 18, 413–430. https://doi.org/10.1016/0168-9274 (95)00068-6. URL: http://linkinghub.elsevier.com/retrieve/pii/0168927 495000686
- Verwer, J.G., 1994. Gauss–Seidel iteration for stiff ODES from chemical kinetics. SIAM J. Sci. Comput. 15, 1243–1250. https://doi.org/10.1137/0915076.
- Vilà-Guerau de Arellano, J., Patton, E.G., Karl, T., van den Dries, K., Barth, M.C., Orlando, J.J., 2011. The role of boundary layer dynamics on the diurnal evolution of

- isoprene and the hydroxyl radical over tropical forests. J. Geophys. Res. Atmos. 116, D07304. https://doi.org/10.1029/2010JD014857.
- Vilà-Guerau de Arellano, J., Wang, X., Pedruzo-Bagazgoitia, X., Sikma, M., Agustí-Panareda, A., Boussetta, S., Balsamo, G., Machado, L., Biscaro, T., Gentine, P., et al., 2020. Interactions between the amazonian rainforest and cumuli clouds: a large-eddy simulation, high-resolution ecmwf, and observational intercomparison study. J. Adv. Model. Earth Syst. 12, e2019MS001828.
- Wei, D., Fuentes, J.D., Gerken, T., Chamecki, M., Trowbridge, A.M., Stoy, P.C., Katul, G. G., Fisch, G., Acevedo, O., Manzi, A., et al., 2018. Environmental and biological controls on seasonal patterns of isoprene above a rain forest in central Amazonia. Agric. For. Meteorol. 256, 391–406.
- Wei, D., Fuentes, J.D., Gerken, T., Trowbridge, A.M., Stoy, P.C., Chamecki, M., 2019. Influences of nitrogen oxides and isoprene on ozone-temperature relationships in the Amazon rain forest. Atmos. Environ. 206, 280–292.
- Whalley, L., Edwards, P., Furneaux, K., Goddard, A., Ingham, T., Evans, M., Stone, D., Hopkins, J., Jones, C.E., Karunaharan, A., et al., 2011. Quantifying the magnitude of a missing hydroxyl radical source in a tropical rainforest. Atmos. Chem. Phys. 11, 7223–7233.
- Wolfe, G.M., Thornton, J.A., 2011. The chemistry of atmosphere-forest exchange (CAFE) model Part 1: model description and characterization. Atmos. Chem. Phys. 11, 77–101. https://doi.org/10.5194/acp-11-77-2011. URL: http://www.atmos-chem-phys.net/11/77/2011/.
- Yáñez-Serrano, A.M., Nölscher, A.C., Bourtsoukidis, E., Gomes Alves, E., Ganzeveld, L., Bonn, B., Wolff, S., Sa, M., Yamasoe, M., Williams, J., et al., 2018. Monoterpene chemical speciation in a tropical rainforest: variation with season, height, and time of dayat the Amazon tall tower observatory (ATTO). Atmos. Chem. Phys. 18, 3403–3418.